sorption in the wavelength region shorter than 400 mμ is due to the charge-transfer band of the complex between molecular bromine and toluene,[15] and a shoulder at 405 mμ is due to the characteristic absorption band of molecular bromine. Within 10 μsec after the flash, there is a slight increase of absorption in the region 570–650 mμ, and the decrease of the concentration of molecular bromine was rather slight. Then, most of the disappearance of bromine takes place in the dark period. About one-half of molecular bromine disappeared at 15 μsec after the flash. This fact confirms that almost all the bromine disappeared by the secondary processes initiated by the flash excitation. Until now, the halogenation reaction mechanism has been studied only by the kinetic analysis. Our result is an example directly showing that the halogenation is based on the chain reaction such as shown above.

We have also found that such a chain reaction did not occur when aerated solutions were used, indicating that the benzyl radical as an intermediate in the chain reaction reacts with oxygen dissolved in the solutions.[16]

We have also studied the flash photolysis of a solution of bromine in benzene in the presence of $10^{-2}$ *M* toluene. Even in this system, an absorption band similar to that of the charge-transfer complex between atomic bromine and benzene appeared at about 10 μsec after the flash irradiation. All of the bromine molecules disappeared with a single flash irradiation. The rate of the decrease of concentration of molecular bromine was nearly equal to that obtained in liquid toluene. If the mechanism described above for the chain reaction is true, this result suggests that reaction 4, which is diffusion controlled, should be the rate-determining step. Benzyl radical formed has a strong absorption in the near-ultraviolet region, but its absorption in the visible region is very weak.[17] In the present experiment, the measurement in the ultraviolet region was very difficult, owing to the strong absorption of the halogen and the reaction products. The concentration of the benzyl radical during the chain reaction must be very low, and it is reasonable that we did not find any absorption due to the benzyl radical in the visible region.

(15) R. M. Keefer and L. J. Andrews, *J. Am. Chem. Soc.*, 72, 4677 (1950).

(16) According to the result by Strong, the amount of iodine atom formed in various organic solvents was not affected by the presence of oxygen (see ref 8).

(17) G. Porter and B. Ward, *J. Chim. Phys.*, 1517 (1964).

# Electrogenerated Chemiluminescence. III. Intensity–Time and Concentration–Intensity Relationships and the Lifetime of Radical Cations of Aromatic Hydrocarbons in N,N-Dimethylformamide Solution

**Stephen A. Cruser and Allen J. Bard**[1]

*Contribution from the Department of Chemistry, The University of Texas at Austin, Austin, Texas 78712.* *Received June 5, 1968*

**Abstract:** The intensity–time behavior observed during electrogenerated chemiluminescence (ECL) for multiple cycles and for cases where one of the radical ions is unstable has been investigated. Working curves, obtained by digital computer simulation, are presented which allow determination of the rate constants for the decomposition of the radical ions. The half-lifes of the cation radicals of 9,10-diphenylanthracene, 1,3,6,8-tetraphenylpyrene, and rubrene were determined experimentally. The maximum ECL intensity, obtained by passing alternating current through the cell, was, in all cases, a linear function of the concentration of the electroactive species.

Most of the previous reports of electrogenerated chemiluminescence (ECL) have dealt with proposed mechanisms and with observation of the phenomenon itself.[2] Little attention has been paid to quantitative treatments of the problems of mass transfer and kinetics during ECL, particularly upon repeated cycling. Feldberg[3] has derived, using digital computer techniques, theoretical equations relating, quantitatively, the light intensity produced in ECL to the current, time, and kinetic parameters using a double potential step mode of generation and assuming the light-producing reaction is an anion-radical–cation-radical annihilation followed by radiative decay. Experimental verification of Feldberg's equations has been reported for the ECL of rubrene, under conditions where both ion radicals are stable for the duration of the experiment.[4,5]

We report here an extension of Feldberg's digital simulation technique to allow for additional reactions of the ion radicals and for multiple cycles. In this case, the theoretical intensity–time curves are indicative of the stability of the radicals involved in the annihilation reaction. Several aromatic hydrocarbons have been investigated and the half-lives of the radical cations

(1) To whom correspondence and requests for reprints should be directed.

(2) T. Kuwana, "Electroanalytical Chemistry," Vol. I, A. J. Bard, Ed., Marcel Dekker, Inc., New York, N. Y., 1966, Chapter 3, and references contained therein.

(3) (a) S. W. Feldberg, *J. Am. Chem. Soc.*, **88**, 390 (1966); (b) *J. Phys. Chem.*, 70, 3928 (1966).

(4) J. Chang, D. M. Hercules, and D. K. Roe, *Electrochim. Acta*, **13**, 1197 (1968).

(5) R. E. Visco, and E. A. Chandross, *ibid.*, **13**, 1187 (1968).

were determined. The maximum intensity during ECL of these compounds was shown to be a linear function of the concentration of the electroactive species.

## Experimental Section

Rubrene, 9,10-diphenylanthracene (DPA), and 1,3,6,8-tetraphenylpyrene (TPP) were obtained from Aldrich Chemical Co. and were vacuum sublimed before use. Anthracene, obtained from Matheson Coleman and Bell, was purified as described in a previous paper.[6] Polarographic grade tetra-*n*-butylammonium perchlorate (TBAP), obtained from Southwestern Analytical Chemicals, Austin, Texas, was used as the supporting electrolyte in all experiments. It was vacuum dried at a temperature of 85° for 24 hr and stored in a desiccator over anhydrous magnesium perchlorate. The solvent, N,N-dimethylformamide (DMF), from Matheson Coleman and Bell, was purified by the same procedure as that reported previously.[6]

Two different types of electrolysis cells were employed. Cell 1, consisting of two coiled platinum helices sealed into the walls of a standard taper joint (24/40), was used in all alternating current measurements as well as in recording the fluorescence and ECL spectra. This cell was provided with an adapter with a high-vacuum stopcock so that a low pressure could be maintained over the solution. Cell 2 was of conventional electrochemical design and was used for cyclic voltammetric and cyclic potential step measurements. The working electrode was a platinum disk with an apparent electrode area of 0.03 $cm^2$. The platinum auxiliary electrode was separated from the bulk solution by means of a compartment closed at the bottom with a medium porosity glass frit. An aqueous saturated calomel electrode (sce) with a 3% 1 *M* potassium nitrate salt bridge with a medium porosity sintered-glass disk closing the end immersed in the electrolysis solution was used as the reference electrode.

Dissolved gases were removed from the electrolysis solution using a freeze–pump–thaw method on a vacuum line much like that previously described.[7] When the three-electrode cell was used, helium (99.995% purity) was introduced into the cell in order to insert the reference electrode after the contents of the cell had been deaerated. This helium had passed successively through anhydrous magnesium perchlorate, copper turnings heated to 350°, and a trap cooled to liquid nitrogen temperatures to remove any traces of water and organic impurities. The cell was then sealed off to prevent contamination of the test solution by air. This technique proved quite satisfactory for both ECL and electrochemical experiments.

All emission measurements were made using either an Aminco-Bowman spectrophotofluorometer (RCA 1P21 photomultiplier tube) or a Dumont 6467 photomultiplier tube with the output connected to an oscilloscope. Rather wide slit widths were employed with the spectrophotofluorometer to increase sensitivity. The Dumont phototube was used because the response time of the Aminco amplifier was relatively slow (approximately 0.3 sec). It, with its associated bank of resistors, was positioned in one end of a black wooden box, and the cell was placed directly in front of the tube through a hole in the top of the box. The entire optical assembly, including the cell, was then covered with a black cloth to prevent external light from leaking into the photomultiplier tube. A Kepco model regulated dc power unit (General Electric) supplied the necessary voltage to the phototube. The emission spectra and intensity–time curves were recorded either on a Moseley Model 7005A X-Y recorder or on a Tektronix Type 564 storage oscilloscope.

The cyclic voltammetric and cyclic potential step behavior studies utilized a Wenking Model 61-RH potentiostat in conjunction with a Wavetek Model 114 function generator and associated switching and triggering circuitry.

Sinusoidal ac for two-electrode experiments was obtained from a 6.3-V filament power supply with an autotransformer as a voltage divider.

Computer calculations were done on a Control Data Corp. (CDC) 6600 computer.

## Results

**Theoretical Treatment.** The following over-all mechanism is assumed to hold.

$$R + e \longrightarrow R^- \quad \text{(reduction at the electrode surface)} \quad (1)$$

$$R \longrightarrow R^+ + e \quad \text{(oxidation at the electrode surface)} \quad (2)$$

$$R^- \longrightarrow R + 2e \quad (3)$$

$$R^+ (+Z) \xrightarrow{k} X \quad \text{(decay of the cation radical)} \quad (4)$$

$$R^- + R^+ \xrightarrow{k_a} R^* + R$$

(annihilation reaction in the diffusion layer) (5)

$$R^* \xrightarrow{k_r} R + h\nu \quad \text{(radiative decay of the excited singlet)} \quad (6)$$

These equations are similar to those used by Feldberg,[8] except that the possibility of decomposition of the cation radical in a pseudo-first-order reaction is considered in reaction 4. Since for most aromatic hydrocarbons in most solvents used for ECL either the anion or cation radical is unstable, it will be generally necessary to include this reaction. Because studies reported here concern ECL in DMF, in which cation radicals are unstable but anion radicals are very stable, the above sequence, assuming generation of the anion radical first, and then reversal, is treated. Obviously exactly the same treatment will apply in solutions where the anion radical is unstable, assuming an initial generation of the cation.

The following assumptions were made in the treatment: (1) the rate of the annihilation reaction, eq 5, was diffusion controlled; (2) the radiative decay of R*, reaction 6, was very fast; (3) the involvement of excimers and triplets was not important; and (4) the involvement of other oxidizing and reducing species either present in solution or generated electrochemically was not important. Since electron transfer and radiative decay of the singlet have been shown to be very fast (rate constant of the order of $10^8$ $sec^{-1}$), the first two assumptions are probably valid. Nonradiative decay of R* is accounted for by modifying the calculated intensity by a factor $\Phi$ representing the fraction of excited species undergoing radiative decay. Inclusion of self-quenching would make $\Phi$ a concentration-dependent parameter. Some evidence reported later suggests that self-quenching is probably not important in the reactions considered here. This method of inclusion of nonradiative reactions in the scheme is the same as that described by Feldberg.[8] Since most intensity and spectral measurements in ECL involve repetitive cycling of potential (or applied sinusoidal ac), we have also extended the case to include this possibility.

The above reaction scheme was treated using the digital simulation approach, which is particularly applicable to solving problems involving nonlinear partial differential equations. In this approach the solution is considered to be an array of small homogeneous volume elements parallel to the electrode surface. Stepping the potential to diffusion-limited plateaus of the current–potential curves corresponds to decreasing the concentration of the electroactive species to zero in the volume element adjacent to the electrode. Linear diffusion, the only mode of mass transfer considered here, is treated by transfer of material from one volume element to the next, according to the difference equation form of Fick's equation. Kinetic calculations involve variations of concentrations within each volume element. A complete description of the particular program used in this study has appeared elsewhere;[8] a

(6) L. R. Faulkner and A. J. Bard, *J. Am. Chem. Soc.*, **90**, 6284 (1963).

(7) K. S. V. Santhanam and A. J. Bard, *ibid.*, **88**, 2669 (1966).

(8) S. A. Cruser, Ph.D. Dissertation, The University of Texas at Austin, Austin, Texas, 1968.

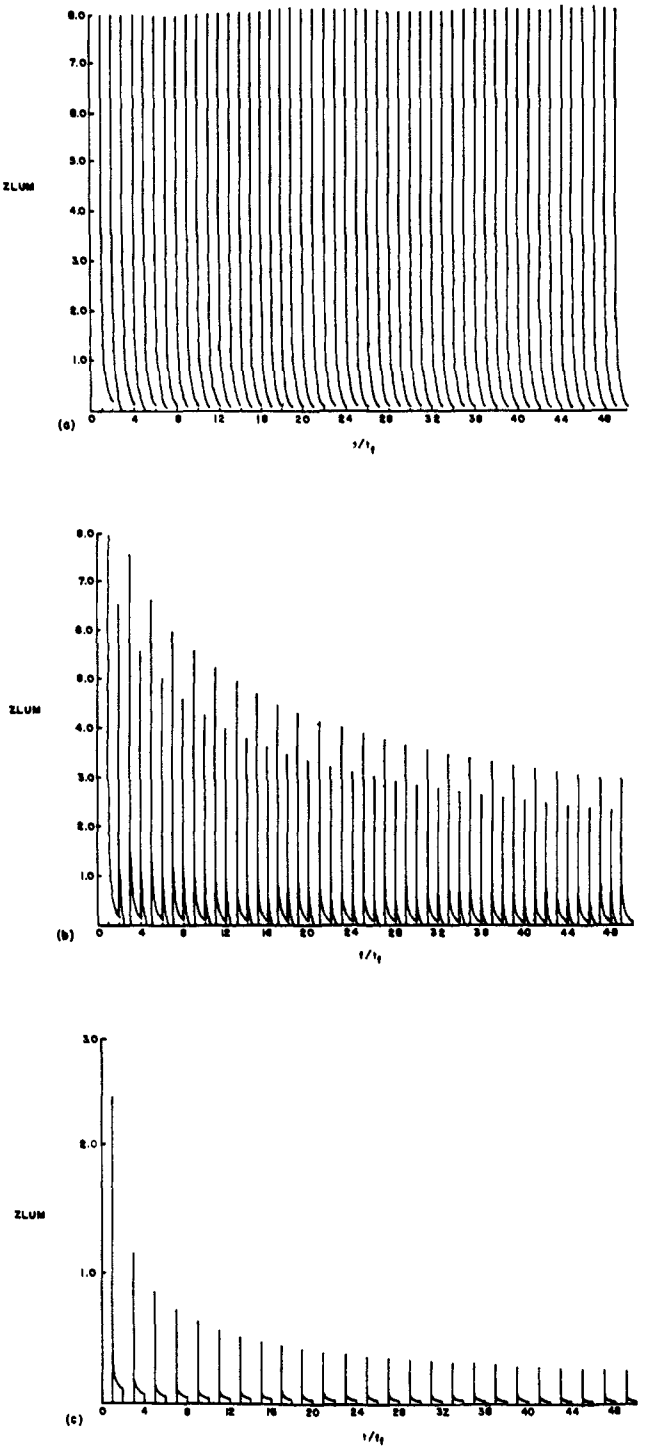


Figure 1. Theoretical computer plots of ZLUM, the intensity parameter, *vs.* $t/t_f$: (a) $kt_f = 0.0$, (b) $kt_f = 1.0$, (c) $kt_f = 100.0$.

brief discussion of the method and techniques is given in the Appendix.[9]

**Intensity–Time Curves.** Computer calculations were made for various values of the dimensionless rate constant parameter, $kt_f$, where $k$ is the pseudo-first-order rate constant for the cation decay (reaction 4) in second$^{-1}$ and $t_f$ is the duration of the first half-cycle in seconds. ZLUM (which corresponds to Feldberg's $\omega^3$) is the dimensionless intensity parameter, defined as

$$\text{ZLUM} = It_f^{1/2}/C^*A\Phi D^{1/2} \quad (7)$$

where $I$ is the radiation intensity in moles of photons/sec, $C^*$ is the bulk concentration of the electroactive species in moles/cm$^3$, $A$ is the electrode area in cm$^2$, $\Phi$ is the quantum efficiency, and $D$ is the diffusion coefficient in cm$^2$/sec.

The computer output depicted in Figure 1a represents a plot of ZLUM *vs.* $t/t_f$ ($t$ is the total elapsed time) for $kt_f = 0$; *i.e.*, the reaction $R^+$ forming X does not occur. This corresponds to the case treated by Feldberg,[3] extended to multiple cycles. Note that two radiation pulses of equal intensity, decaying with time during the potential step, occur per cycle. Note that because the over-all sequence of reactions regenerates R, all radiation pulses on repetitive cycling are the same, so that this type of ECL response can be taken as characteristic of electrogenerated anion and cation radicals both of which are stable during the duration of the potential step. When a finite rate constant for reaction 4 is introduced, the intensity which occurs when $R^-$ is produced on the second reversal is smaller than that obtained on the first reversal (Figure 1b). Moreover, since the reaction sequence now involves loss of R in the vicinity of the electrode, the over-all envelope of intensity peaks decays. When $k$ becomes sufficiently large, only one pulse per cycle is obtained, since no $R^+$ is available during odd-numbered cycles to react with electrogenerated $R^-$ (Figure 1c). Note, however, that even for very fast decay of $R^+$, radiation is obtained upon electrogeneration of $R^+$, since the fast reaction with $R^-$ can compete successfully with the decay of $R^+$.

Three methods were employed to relate the theoretical results to experiment. In the first method the integrated intensity, *i.e.*, area, was calculated for each curve. The ratio of the area of each even-numbered peak to that of the preceding odd-numbered peak was constant, along the entire envelope, for a particular value of the parameter $kt_f$, varying from 1.0 to 0 as the value of $kt_f$ increased. A plot of this intensity ratio *vs.* log $kt_f$ is shown in Figure 2. Since all of the parameters in ZLUM, except the intensity, are constant for a given experiment, the stability of the cation and $k$ can be determined by plotting the experimental ratios of these two peaks for various frequencies and by fitting the data to the working curve. In a second method of data treatment, a family of working curves can be constructed by plotting the intensity ratio of each of the larger peaks of the over-all envelope (normalized to the first large intensity peak) *vs.* the cycle number, for different values of $kt_f$. Figure 3 represents this family of theoretical working curves. The experimentally observed decay envelope can be compared to these to obtain $k$. Finally only the first intensity–time curve, obtained for the first reversal, can be employed yielding plots analogous to those of Feldberg.[3] Assuming the annihilation reaction proceeds at an infinite rate, a normalized plot of log ZLUM *vs.* $(t_r/t_f)^{1/2}$ for various values of $kt_f$ yielded the data shown in Figure 4a. In this plot $t_r = t - t_f$, so that $t_r$ is the time at any point during the second half-cycle. Figure 4b shows the slope of each of the lines in 4a plotted against the value of $kt_f$. The slope decreases from the value of $-1.45$[3] as $kt_f$ increases. The second and third method of data treatment have the advantage

(9) For a complete discussion of the technique of digital simulation in electrochemical problems, see S. W. Feldberg in "Electroanalytical Chemistry," Vol. III, A. J. Bard, Ed., Marcel Dekker, Inc., New York, N. Y., 1969.

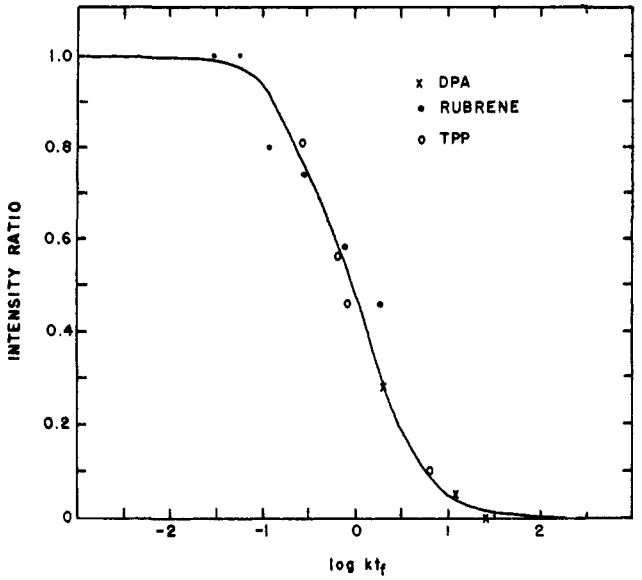


Figure 2. Theoretical plot of the integrated intensity ratio *vs.* log $kt_f$. This is a working curve for the evaluation of the rate constant, $k$. The experimental fit of DPA, rubrene, and TPP is also presented.

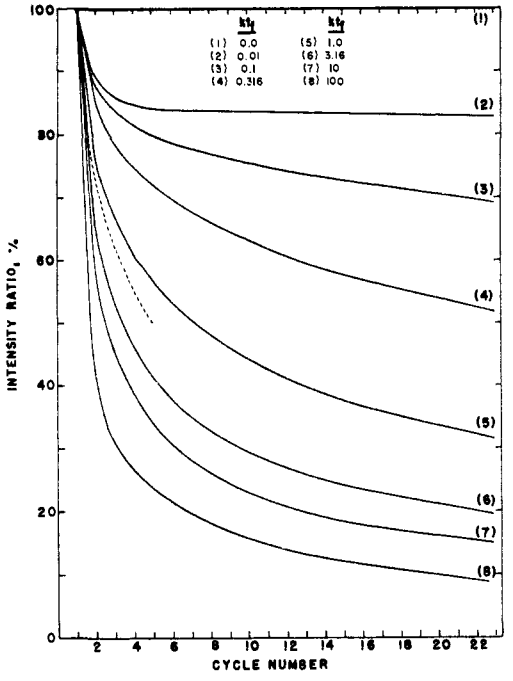


Figure 3. Plot of the integrated intensity ratio (normalized to the first intensity peak) *vs.* cycle number for various values of $kt_f$. The dashed line represents a plot of this behavior for TPP.

of requiring only one peak per cycle for the determination of R, while the first method may be advantageous when it is more convenient to observe later cycles than the first.

**Intensity–Time Studies.** The theoretical equations were tested by investigating the ECL of diphenylanthracene (DPA), rubrene (R), and tetraphenylpyrene (TPP) under cyclic potential-step conditions. In all cases the cyclic voltammetric behavior of the compound was investigated first and the potentials for ECL experiments were chosen on this basis. All solutions in these experiments were DMF containing 0.1 *M* TBAP. The working electrode was a platinum disk.

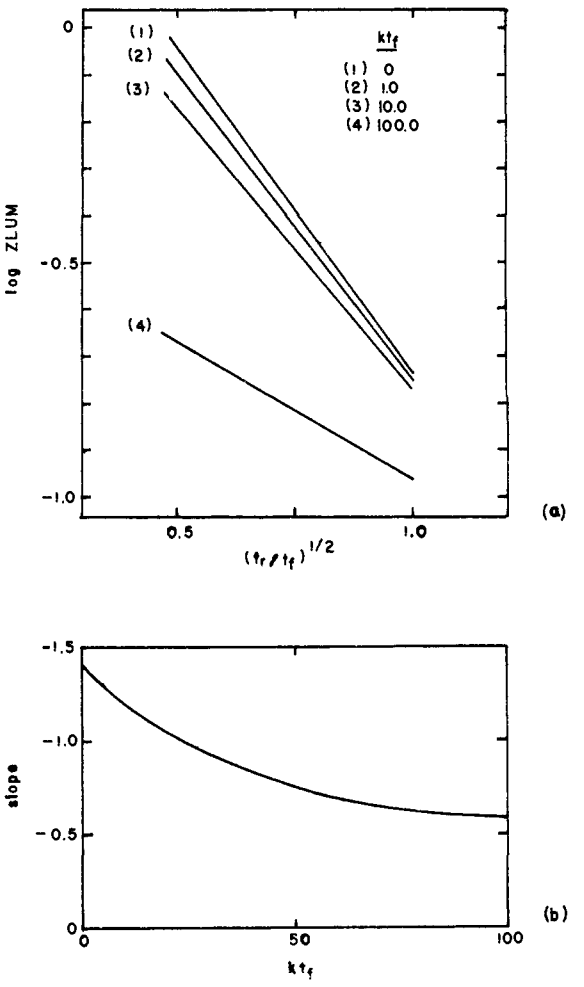


Figure 4. (a) Plot of log ZLUM *vs.* $(t_r/t_f)^{1/2}$ for various values of $kt_f$. (b) Plot of the slope of each of the lines in 4a *vs.* $kt_f$. Only the decay of the initial intensity pulse is considered in this treatment of the data.

Cyclic voltammetric reduction of DPA shows a reversible one-electron reduction to the stable radical[7] at −1.89 V *vs.* sce. The reduction to the dianion, which quickly undergoes a following protonation reaction, occurs at −2.6 V. Oxidation of DPA occurs at +1.35 V *vs.* sce. The oxidation and no reversal (reduction) peak is observed at scan rates of 0.255 V/sec. The intensity–time behavior of DPA with cyclic potential steps between −1.89 and +1.35 V *vs.* sce (reduction first) is shown in Figure 5a and 5b for frequencies of 5 and 60 cps, respectively. Note at 5 cps only one intensity peak per cycle is observed, with a rather rapid decay of the intensity envelope. At 60 cps a small peak appears on the odd-numbered (reduction) steps, and a much slower decay of intensity is observed. This behavior corresponds closely to that shown in Figure 1b and 1c. The relative areas of the reduction to oxidation intensity curves at 5, 10, and 60 cps were 0, 0.05, and 0.28, respectively. When these data are fitted to the working curve in Figure 2, a rate constant for the decay of $DPA^+$ of about 225 $sec^{-1}$ is obtained. The rate constant could also be obtained by analysis of the first intensity pulse shown in Figure 5c, by the method suggested in Figure 4. A plot of log $I$ *vs.* $(t_r/t_f)^{1/2}$ based on the first pulse had a slope of −0.87, corresponding to a rate constant of about 140 $sec^{-1}$.

Rubrene exhibits reversible reduction and oxidation waves at −1.50 and +1.10 V *vs.* sce, respectively.[10] When the electrode is cycled between these two potentials at different frequencies and the relative areas of the oxidation to reduction peaks are determined, the data shown in Table I are obtained. When these results

**Table I.** Integrated Intensity Ratios for Rubrene and Tetraphenylpyrene at Different Frequencies[a]

| Frequency, cps | Intensity ratio Rubrene[b] | TPP[c] |
|---|---|---|
| 0.25 | 0.46 | |
| 0.50 | 0.58 | |
| 1.0 | 0.74 | 0.10 |
| 2.5 | 0.80 | |
| 5.0 | 1.00 | 0.46 |
| 10.0 | 1.00 | 0.56 |
| 25.0 | | 0.81 |

[a] The solution was 0.10 *M* TBAP in DMF. [b] 0.5 m*M* rubrene, cycled between −1.50 and +1.10 V *vs.* sce. [c] 0.1 m*M* TPP, cycled between −1.83 and +0.95 V *vs.* sce.

were fitted to the working curve (Figure 2), a pseudo-first-order rate constant for the decomposition of rubrene cation was calculated to be approximately 0.56 $sec^{-1}$, corresponding to a half-life of slightly longer than 1 sec. Hercules, *et al.*,[10] estimated, using cyclic voltammetry, that the half-life of rubrene cation was about 3 sec in this medium.

The cyclic voltammetric behavior of 0.1 m*M* TPP shows a reversible reduction wave at −1.83 V *vs.* sce and an oxidation at +0.95 V *vs.* sec. The intensity–time behavior upon cyclic potential steps is similar to that for DPA, and the resulting integrated intensity ratios are given in Table I. These results, fitted to the working curve in Figure 2, yield a rate constant for the decomposition of $TPP^+$ of 13 $sec^{-1}$. An alternate approach is to fit the envelope of the odd-numbered intensity pulses to a working curve such as in Figure 3; the rate constant calculated by this method is 19 $sec^{-1}$.

**Concentration–Intensity Studies.** The theoretical treatments predict that ZLUM is a constant at a given value of $kt_f$, so that, by eq 7, the intensity should be proportional to concentration of the hydrocarbon. This prediction was tested by observing ECL in the two-electrode cell with a constant applied 60-cycle sinusoidal voltage. Although these conditions do not correspond exactly to those of the potential-step experiments, they are much simpler to apply in practice and allow more convenient cell design for placement in the spectrophotofluorometer. By proper choice of the magnitude of the alternating voltage (see below), so that the potential of the electrodes varies between the diffusion plateaus for the cathodic and anodic processes, the conditions are close to those in the potential-step experiments. Portions of a stock solution of the aromatic hydrocarbon in DMF were diluted to make up solutions of different concentrations. Each contained at least a 100-fold excess of supporting electrolyte (TBAP) to decrease the solution resistance and to ensure that mass transfer of ions was predominantely by diffusion. In each case the upper concentration limit investigated was governed by the maximum solubility limit of the hydrocarbon in DMF and the minimum concentration limit was that from which no light emission could

(10) D. M. Hercules, R. C. Lansbury, and D. K. Roe, *J. Am. Chem. Soc.*, **88**, 4578 (1966).

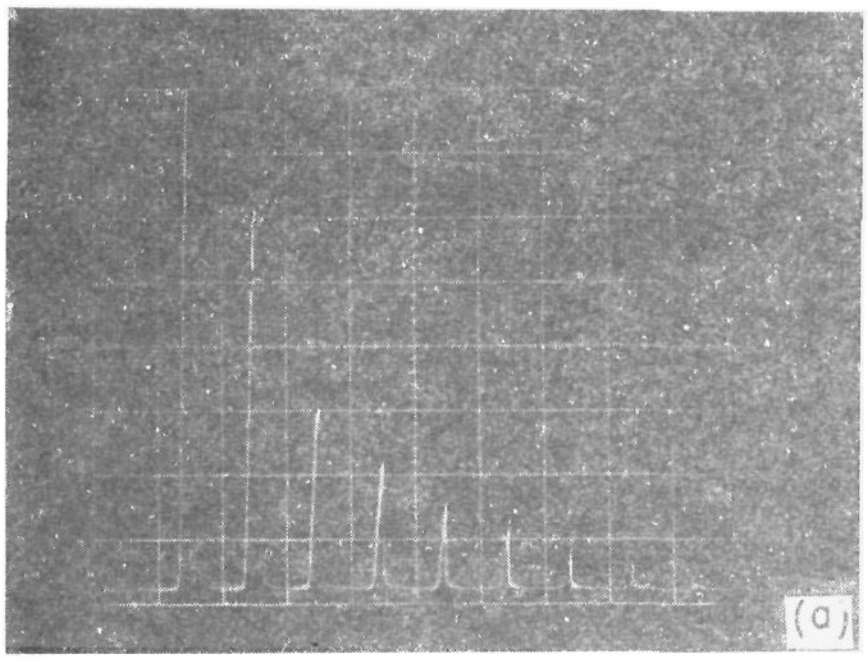


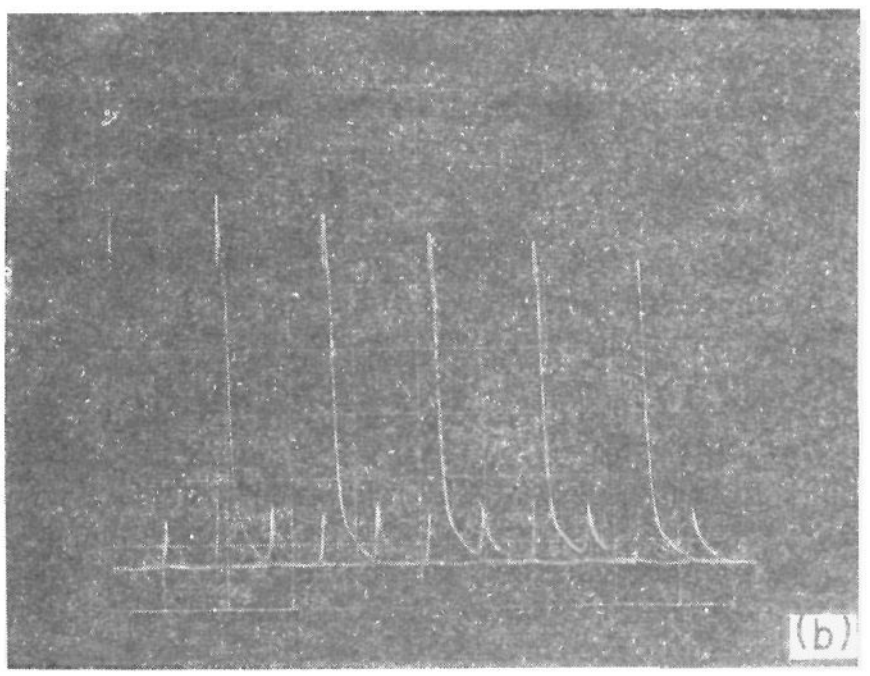


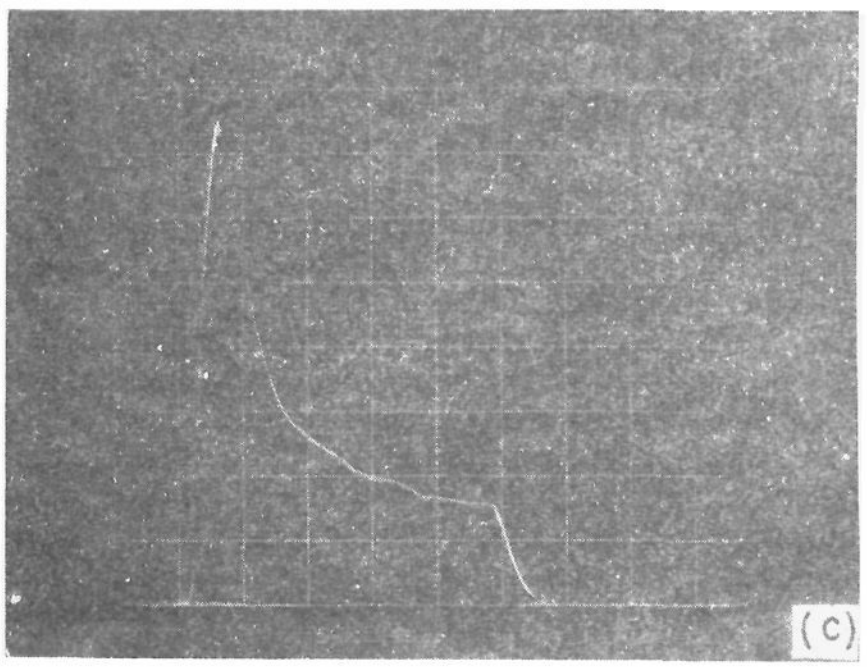


Figure 5. Experimental intensity–time behavior for 1 m*M* DPA in DMF obtained by potentiostating between −1.89 and +1.35 V *vs.* sce. The Dumont photomultiplier tube and an oscilloscope were used at the optical assembly. In (a) the frequency was 5 cps (time axis represents 0.2 sec/division); in (b) the frequency was 60 cps (time axis represents 10 msec/division); and in (c) the frequency was 2 cps (time axis represents 50 msec/division).

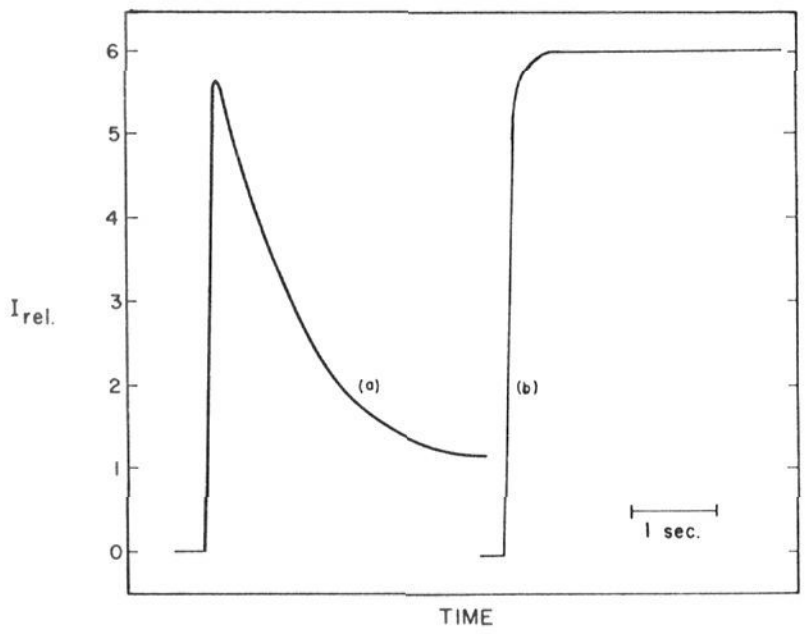


Figure 6. Experimental intensity–time curves using the Aminco–Bowman spectrophotofluorometer: (a) 10 m*M* DPA in DMF with an applied voltage of 6.3 V; (b) 0.25 m*M* rubrene in DMF with an applied voltage of 2.5 V.

be detected with the spectrophotofluorometer. All solutions were vacuum degassed, using several freeze–pump–thaw cycles, and sealed off prior to carrying out the intensity measurements. The cell was placed inside the spectrophotofluorometer in a reproducible fashion with the electrodes aligned colinearly with the monochromator entrance slits to give the maximum intensity. The experimental procedure consisted of recording an intensity–time (*I–t*) curve at a given applied voltage, stirring the solution, and waiting 2 min before recording another *I–t* curve. The relative intensity was measured as an average of at least three experimental trials.

The compounds DPA, rubrene, and TPP exhibit type I ECL behavior;[11] that is, the ECL emission wavelength maximum for the compound is identical with the emission wavelength maximum for fluorescence of that compound. Anthracene exhibits type II behavior, exhibiting, in addition to emission at the fluorescence maximum, a longer wavelength ECL emission. This band has recently been attributed to the generation and subsequent emission of anthranol.[6] For each compound all *I–t* curves were recorded at the fluorescence emission wavelength maximum.

A typical *I–t* curve resulting from the application of an alternating current to the cell containing a solution of either anthracene, DPA, or TPP is shown in Figure 6a. Zero time corresponds to the moment the current is switched on; *i.e.*, the initial intensity spike begins at zero time. Because of the slow response time of the spectrophotofluorometer amplifier employed in the studies, this curve represents the average, as opposed to the instantaneous, intensity with time behavior or the envelope of the instantaneous *I–t* curve, such as in Figure 5b. As shown before the average intensity goes through a peak and then decays to a steady-state value. The *I–t* behavior for rubrene was different from that of the other compounds. Between 1.9 and 3.6 V applied the intensity rises to a constant value (Figure 6b), as expected for a system in which both anion and cation radicals are stable, where the envelope of instantaneous curves such as Figure 1a is obtained. If the applied

(11) A. J. Bard, K. S. V. Santhanam, S. A. Cruser, and L. R. Faulkner, "Fluorescence," G. G. Guilbault, Ed., Marcel Dekker, Inc., New York, N. Y., 1967, Chapter 14.

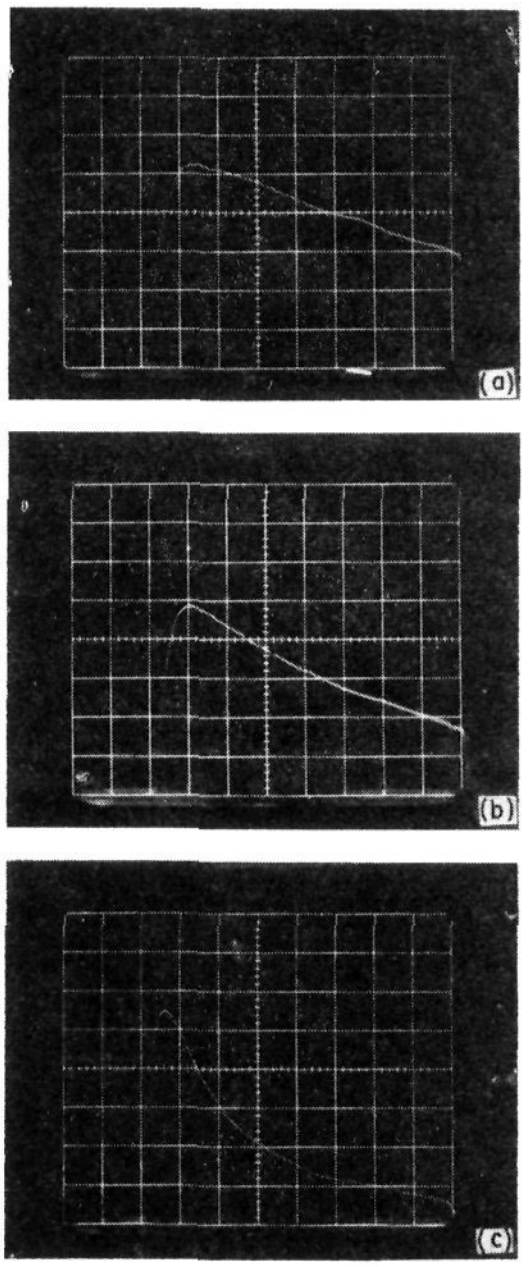


Figure 7. Experimental intensity–time curves for 0.5 m*M* rubrene in DMF. The time axis represents 0.5 sec/division. In (a) the applied voltage was 4.0 V; in (b) the applied voltage was 4.2 V; and in (c) the applied voltage was 4.5 V.

voltage was increased further, the average intensity began to decay with time. Finally the intensity began to peak and the *I–t* behavior looked much like those systems previously described (Figure 7). This behavior can be ascribed to an applied voltage of sufficient magnitude to generate the dianion or products from the solvent or supporting electrolyte system which probably react with the cation radical and thus prevent it from participating in the light-producing reaction. Indeed the instantaneous *I–t* curves show equal intensities for each cycle when the potential steps do not fall into the background region. When potential steps into the background are employed, the instantaneous *I–t* curves show behavior characteristic of decomposition of the radical ions.

The effect of varying the magnitude of the alternating voltage for several of the concentrations of anthracene is shown in Figure 8. As the magnitude of the applied voltage was increased, the peak average intensity increased until finally a constant limiting value was obtained. This probably corresponded to the application of a voltage sweep of sufficient magnitude to cause the potential to step to the limiting current regions of the current–potential curve. Further increase of the voltage led to a sharp decrease in the peak intensity. Again this was probably caused by the electrochemical generation of the anthracene dianion or products from the solvent or supporting electrolyte which react with the relatively unstable cation radical.

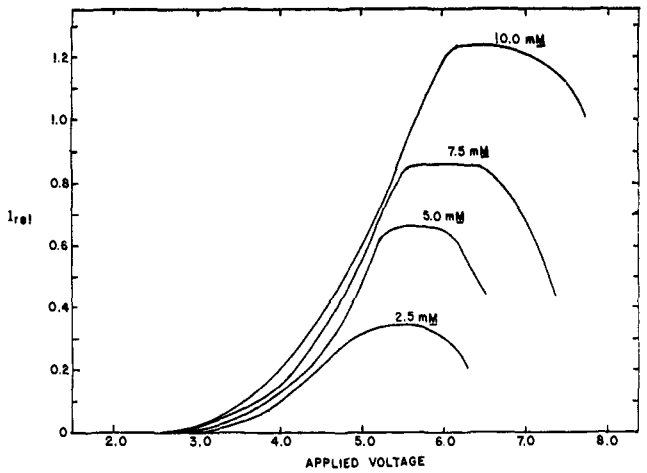


Figure 8. Effect of varying the magnitude of the applied voltage on the intensity for several concentrations of anthracene in DMF.

The concentration–intensity relationship was obtained by adjusting the applied voltage to the limiting region value for each concentration and measuring the maximum peak intensity. In all cases the maximum intensity was a linear function of the concentration. Table II presents the concentration–intensity data for each compound investigated along with a least-squares analysis of the points. The slope of the concentration–intensity line is a function of photomultiplier response, $\Phi$, $A$, $D$, and the averaged value of ZLUM. The slope and total light output will be smaller for smaller values of $\Phi$ and for larger values of the rate constant for decay of the radical ions. The trend in slopes shown in Table II parallels the stabilities of the cation radical, although variations in $\Phi$ among the different compounds must also be important.

**Table II.** Concentration–Intensity Relationship[a]

| Concentration, m$M$ | Peak intensity | Concentration, m$M$ | Peak intensity |
|---|---|---|---|
| Anthracene | | Rubrene | |
| 10.70 | 1.21 | 0.50 | 17.60 |
| 8.05 | 0.84 | 0.35 | 12.30 |
| 5.35 | 0.65 | 0.25 | 9.20 |
| 2.68 | 0.34 | 0.10 | 3.20 |
| 1.35 | 0.08 | 0.05 | 1.70 |
| 0.67 | 0.06 | 0.01 | 0.38 |
| | | 0.001 | 0.04 |
| $I = (0.11 \pm 0.03)C$[b] | | $I = (35.66 \pm 0.14)C$[b] | |
| DPA | | TPP | |
| 10.00 | 6.58 | 0.157 | 0.199 |
| 5.00 | 3.38 | 0.104 | 0.135 |
| 2.50 | 1.53 | 0.078 | 0.103 |
| 1.00 | 0.59 | 0.052 | 0.066 |
| 0.80 | 0.52 | 0.026 | 0.033 |
| 0.56 | 0.31 | | |
| 0.28 | 0.17 | | |
| $I = (0.66 \pm 0.04)C$[b] | | $I = (1.28 \pm 0.01)C$[b] | |

[a] The solution was 0.10 $M$ TBAP in DMF for hydrocarbon concentrations of 1 m$M$ or less. For higher concentrations, the solution was 1 $M$ TBAP. [b] $I$ = intensity (photomultiplier output) at fluorescence wavelength maximum; $C$ = concentration. Standard deviation of the slope of least-squares line forced through origin is given.

The linearity of the concentration–intensity behavior of anthracene at concentrations above 1 m$M$ is particularly interesting, since the fluorescence emission in this region is decidedly nonlinear due to self-quenching.[12] The absence of self-quenching effects in the ECL emission probably arises because the annihilation reaction occurs in the diffusion layer near the electrode where the concentration of parent hydrocarbon is small. Indeed the linear concentration–intensity behavior for all of the compounds suggests that $\Phi$ is not a function of concentrations, and that self-quenching is not important in the observed ECL emission.

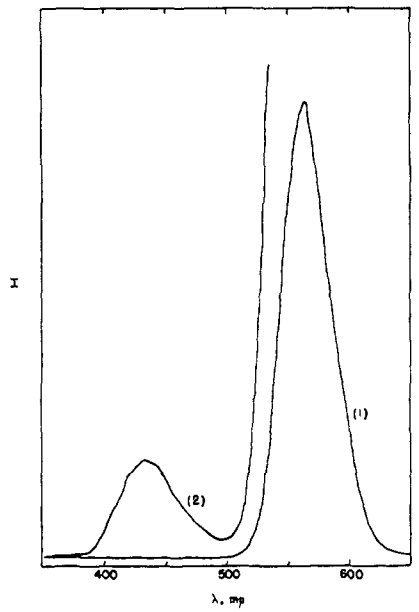


Figure 9. ECL spectra of a mixture of DPA and rubrene. In curve 1 the applied voltage was 2.2 V, and in curve 2 the applied voltage was 6.0 V.

Preliminary experiments on the intensity–concentration relationship were performed on a mixture of DPA and rubrene. These compounds were chosen because they are both type I compounds and their maximum fluorescence bands are separated by about 140 m$\mu$, so that the individual emission bands of each could be observed. The ECL spectrum of a DPA–rubrene mixture in DMF with TBAP as the supporting electrolyte is shown in Figure 9. The rubrene ECL spectrum (curve 1) was recorded by applying 2.2 V across the cell. No DPA emission occurred at this applied voltage. As the voltage was increased above 3.8 V, DPA emission began to appear. Curve 2 was recorded at an applied voltage of 6.0 V. The average intensity–time behavior at the maximum emission wavelength of each component in the mixture was exactly the same as in the single component systems. Rubrene emission was constant up to a certain applied voltage, while DPA emission always passed through a peak intensity and decayed with time.

To determine the relative intensity for each substance, the emission wavelength was first adjusted to 567 m$\mu$, the maximum emission wavelength for rubrene in DMF, and the relative intensity was measured with increasing applied voltage. The maximum intensity was taken, just as before, with the magnitude of the applied voltage set at a point just prior to where the $I$–$t$ curve began to decay. Then the emission wavelength was adjusted to

(12) A. Dammers de Klerk, *Mol. Phys.*, **1**, 141 (1958).

429 mμ, the maximum emission wavelength for DPA in DMF, and the intensity was measured as before. The maximum intensity was taken with the applied voltage adjusted to the limiting portion of the intensity-applied voltage curve. Table III presents the intensity values

Table III. Relative Intensity for Different Concentrations of a Mixture of Rubrene and 9,10-Diphenylanthracene[a]

| Concentration, m*M* | | Peak intensity | |
|---|---|---|---|
| Rubrene | DPA | Rubrene | DPA |
| 0.25 | 0.50 | 8.96 | 0.32 |
| 0.25 | 1.00 | 8.96 | 0.60 |
| 0.25 | 2.00 | 8.91 | 1.46 |
| 0.25 | 5.00 | 8.97 | 3.46 |
| 0.25 | 10.00 | 9.07 | 6.57 |
| | $I = (0.66 \pm 0.07)C$ | | |
| 0.001 | 5.00 | 0.036 | 3.46 |
| 0.01 | 5.00 | 0.39 | 3.42 |
| 0.025 | 5.00 | 0.94 | 3.50 |
| 0.05 | 5.00 | 1.73 | 3.43 |
| 0.10 | 5.00 | 3.40 | 3.40 |
| | $I = (34.32 \pm 0.03)C$ | | |

[a] The maximum intensity for each substance was determined by first setting the emission wavelength at that for rubrene and recording the emission due to rubrene with increasing applied voltage. Then the emission wavelength was adjusted to that for DPA and the recording procedure was repeated.

measured for different concentrations of the two components. Note that the slopes of the concentration–intensity lines for DPA in the presence of rubrene and for rubrene in the presence of DPA are almost the same as those for the single-component systems. This implies that the quantum efficiency, Φ, for each process is not altered, and hence energy transfer between the species is not significant.

## Conclusions

A study of the instantaneous *I–t* curves during ECL can provide information about the stability of the electrogenerated radical ions. Because the rapid annihilation reaction competes with the decomposition reaction, rather rapid decomposition rate constants can be determined. For example, ECL results are obtainable for values of $kt_f$ of 100, which corresponds to $k$'s of $10^5$ $sec^{-1}$ for frequencies of 1 kHz. A corollary of this is that ECL is observable even if one of the electrogenerated species is very unstable.

The good correlation of concentration with intensity suggests analytical applications of ECL[13] as a form of solution emission spectroscopy. Although the effects of quenchers and other interferences must still be investigated, the good sensitivity and selectivity, as well as the rather simple apparatus which can be employed, makes further studies worthwhile. Studies of the slopes of the concentration–intensity curves can also provide information about quantum efficiencies and rates of energy transfer. Further studies on these subjects are being made.

**Acknowledgment.** We are indebted to J. T. Maloy and L. R. Faulkner for helpful discussions during the course of the work. The support of the Robert A. Welch Foundation and the National Science Foundation (GP 6688X) is gratefully acknowledged.

(13) S. A. Cruser and A. J. Bard, *Anal. Letters*, **1**, 11 (1967).

## Appendix. An Outline of the Digital Simulation Technique Employed

The solution is considered to be composed of volume elements extending from the electrode into the solution, numbered $J = 1, 2, \ldots$. Initially, the concentrations of all species of interest in each volume element are set equal to their initial values; in the problem here $C_R = C^*$ and $C_{R^-} = C_{R^+} = 0$ for all boxes. It is advantageous in solving problems by digital simulation to work in terms of dimensionless quantities; relative concentrations, $\bar{C}_R$, $\bar{C}_{R^-}$, and $\bar{C}_{R^+}$ are therefore used, where $\bar{C}_R = C_R/C^*$, $\bar{C}_{R^-} = C_{R^-}/C^*$, and $C_{R^+} = C_{R^+}/C^*$. The initial conditions are then

$$\bar{C}_R(J) = 1.0,\ \bar{C}_{R^-}(J) = \bar{C}_{R^+}(J) = 0, \text{ for all } J \quad \text{(A-1)}$$

For the first cycle (reduction of R to $R^-$) the boundary conditions in the box $J = 1$ are

$$\bar{C}_R(1) = \bar{C}_{R^+}(1) = 0 \quad \bar{C}_{R^-}(1) = 1.0 \quad \text{(A-2)}$$

for the first time increment, and

$$\bar{C}_R(1) = \bar{C}_{R^+}(1) = 0$$

$$\bar{C}_{R^-}(1) = \bar{C}_{R^-}'(1) + D_m[\bar{C}_{R^-}'(2) - \bar{C}_{R^-}'(1) + \bar{C}_R'(2) + \bar{C}_{R^+}'(2)] \quad \text{(A-3)}$$

for all other time increments, where the primed concentrations on the right of (A-3) denote those of the preceding time increment. For each time increment the relative concentrations of each species in the other boxes are calculated by considering linear diffusion into and out of each box using the finite difference form of Fick's second law[9]

$$\Delta\bar{C}(J) = D_m[\bar{C}(J+1) - 2\bar{C}(J) + \bar{C}(J-1)] \quad \text{(A-4)}$$

where $\Delta C(J)$ is the change in concentration in box $J$; $D_m = D\Delta t/\Delta x^2$ is a dimensionless parameter based on the diffusion coefficient and the magnitude of the time ($\Delta t$) and distance ($\Delta x$) increments. The concentrations of species undergoing any chemical reaction (in this case $R^+$) are also varied by the finite difference form of the first-order rate law

$$\Delta\bar{C}(J) = XKT\bar{C}(J) \quad \text{(A-5)}$$

where $XKT$ is the dimensionless parameter $k\Delta t$, and $\bar{C}(J)$ is the value of the relative concentration in box $J$ corrected for diffusion. The concentrations are calculated for time increments up to $t_f$.

Upon reversal both R and $R^-$ in box $J = 1$ are oxidized to $R^+$, and $R^+$ diffuses into the box from box $J = 2$, so that the boundary conditions in box $J = 1$ are

$$\bar{C}_R(1) = \bar{C}_{R^-}(1) = 0 \quad C_{R^+}(1) = 1.0 \quad \text{(A-6)}$$

for the first time increment, and

$$\bar{C}_R(1) = \bar{C}_{R^-}(1) = 0$$

$$\bar{C}_{R^+}(1) = \bar{C}_{R^+}'(1) + D_m[\bar{C}_R'(2) + \bar{C}_{R^-}'(2) - \bar{C}_{R^+}(1)] \quad \text{(A-7)}$$

for all other time increments. The concentrations on the right side of (A-7) are those of the preceding time increment. The reaction between $R^+$ and $R^-$ during the second and following cycles is accounted for by examining each box for the presence of both $R^+$ and

$R^-$, and causing complete reaction of these to produce two R's and a photon. The total moles of photons produced in any time increment are used to calculate ZLUM.

These calculations are continued for each time increment until the next reversal occurs.

The program allows calculation of concentration profiles and intensity–time and current–time curves. A complete listing of the FORTRAN program and an explanation of it is available.[8]

The accuracy of the simulation depends upon the number of iterations in each cycle. The results here were obtained with 200 interations per cycle (*i.e.*, 10,000 iterations for the complete 50-cycle output) and gave values for the current–time behavior and concentration profiles during the first potential step which agreed with the known analytical solutions for this case (*e.g.*, the Cotrell equation) to within 0.5%. ECL calculations in the absence of kinetic effects gave results in excellent agreement with those of Feldberg.[3]

# Electrical Conductance of Bolaform Electrolytes in Viscous Solvents. Manganese(II) *m*-Benzenedisulfonate and Manganese(II) 4,4′-Biphenyldisulfonate in Water–Ethylene Glycol Mixtures at 25°[1]

**P. Hemmes[2] and S. Petrucci**

*Contribution from the Department of Chemistry, Polytechnic Institute of Brooklyn, Brooklyn, New York 11201.* *Received August 30, 1968*

**Abstract**: The electrical conductances of the Mn(II) salts of *m*-benzenedisulfonate ($BDS^{2-}$) and of 4,4′-biphenyldisulfonate ($BPDS^{2-}$) have been measured in mixtures of water–ethylene glycol at 25° up to 0.56 and 0.40 mole fraction of glycol, respectively. The data are interpreted by means of the Fuoss–Onsager 1959 equation for conductance. MnBDS is partially associated in the mixtures, while MnBPDS is substantially unassociated. The $a_A$, $a_J$, and $a_K$ (for the associated electrolyte) show a fair consistency. It is shown that the $BPDS^{2-}$ ion frictional coefficient can be calculated theoretically using the hydrodynamic radius of the benzenesulfonate ion and the Perrin rigid elipsoid model.

Bolaform ions[3] are ions whose total charge is split into discrete charges separated by uncharged areas. This is also the structural feature of both synthetic and biological polyelectrolytes. In fact, the bolaform ion may resemble a segment of the chain of a polyion.

The study of the hydrodynamic and kinetic properties of these ions and their interactions and association with the counterions may link the properties of simple and polyelectrolytes. Indeed the behavior of some bolaform ions can still be interpreted by the theories of simple electrolytes.

The study of this class of electrolytes was initiated by Fuoss and his school at Yale University.[3] Rice[4] reexamined the conductance of some diquaternary ammonium salts[3] and demonstrated the validity of the present conductance theories[5] in the analysis of association and hydrodynamic parameters.

Among the bolaform ions the benzenedisulfonate anions and their derivatives are particularly important. Because of the rigidity of the inert frame interposed between the charges, their properties can be sucessfully interpreted in terms of simple geometrical models.

Atkinson and his associates[6] studied the conductance of these electrolytes rather extensively in water as well as in mixtures of water with organic liquids in order to lower the dielectric constant of the medium. In this laboratory it was decided to extend this research to media of higher viscosity, namely water–ethylene glycol mixtures. It was of interest to study the hydrodynamic and thermodynamic properties of these ions and compare them with the simpler ion $SO_4^{2-}$ in these solvents. In particular it was of interest to study the effect of the progressive separation of the charges (going from the $SO_4^{2-}$ to the $BPDS^{2-}$ ion) on the hydrodynamic and association properties of these ions. As counterion Mn(II) was chosen in view of a previous study of $MnSO_4$ in water–glycol at 25°.[7]

## Experimental Part

Mn(*m*)BDS was prepared as described in the literature.[6] It was crystallized twice from conductance water and dried at 105° to the form $MnBDS \cdot 3.5H_2O$ as checked by cation exchange and titration of the acid. MnBPDS was prepared by a similar preparation

(1) This work is part of the thesis of Paul Hemmes in partial fulfillment of the requirements of the Ph.D. degree.

(2) National Science Foundation Kirk Fellow of the Polytechnic Institute of Brooklyn.

(3) R. M. Fuoss and D. Edelson, *J. Am. Chem. Soc.*, 73, 269 (1951).

(4) S. A. Rice and M. Nagasawa, "Polyelectrolyte Solutions," Academic Press, New York, N. Y., 1961.

(5) R. M. Fuoss and F. Accascina "Electrolytic Conductance," Interscience Publishers, New York, N. Y., 1959.

(6) (a) G. Atkinson, M. Yokoi, and C. J. Hallada, *J. Am. Chem. Soc.*, **83**, 1570 (1961); (b) C. J. Hallada and G. Atkinson, *ibid.*, **83**, 3759 (1961); (c) G. Atkinson and C. J. Hallada, *ibid.*, **84**, 721 (1962); (d) G. Atkinson and S. Petrucci, *J. Phys. Chem.*, 67, 337 (1963); (e) *ibid.*, **67**, 1880 (1963); (f) G. Atkinson and S. Petrucci, *J. Am. Chem. Soc.*, **86**, 7 (1964); (g) B. R. Staples and G. Atkinson, *J. Phys. Chem.*, 71, 667 (1967).

(7) S. Petrucci, P. Hemmes, and M. Battistini, *J. Am. Chem. Soc.*, **89**, 5552 (1967).